

Post-fabrication trimming of photonic integrated circuits by local laser oxidation of titanium film

Aleksandr Tronev, Mikhail Parfenov, Sergey Bozhko, Andrey Ionov, Rais Mozhchil, Sergey Chekmazov, Petr Agruzov, Igor Ilichev, Aleksandr Shamrai

Abstract—Local laser oxidation of a thin titanium film is considered as a means for achieving a precise adjustment of absorption coefficient and effective refractive index of dielectric optical waveguides. A fine phase tuning of an operating point and extinction ratio enhancement up to 57 dB were demonstrated on an integrated optical Ti:LiNbO₃ Mach-Zehnder modulator. The technique affects only slightly the dielectric waveguide material and is very promising for a high accuracy permanent trimming of photonic devices based on dielectric waveguides of different material platforms and fabrication technologies.

Index Terms—integrated optics, photonic integrated circuits, optical waveguides, optical device fabrication, post-fabrication trimming, lithium niobate.

I. INTRODUCTION

PHOTONIC integrated circuits (PICs) attract a great attention of both the academic community and industry. In particular, dielectric waveguide based photonic devices have experienced tremendous progress in recent years and show a strong uptrend in different applications such as telecommunications [1], microwave photonics [2], optical sensing [3] and quantum information technologies [4]. Whereas silicon-based photonics is considered as the most promising material platform [5] owing to the low waveguide loss and compatibility to CMOS fabrication processes, other material platforms for dielectric waveguide fabrication are also developing to further extend the capabilities beyond what silicon can offer. They include lithium niobate [6], nitrides [7], diamond [8], tantalum pentoxide [9] and polymers [10].

All the material platforms mentioned above have similar fabrication challenges related to local variations in waveguide dimensions and refractive index due to technological imperfections. This results in deviations of the device performance, which will slightly differ from its ideal design

on a wafer-scale level. It is common practice to actively tune PICs elements by employing the electro-optic [11] and thermo-optic [12] effects, free carrier dispersion [13] or other principles depending on the material platform. This solution has several disadvantages, including a complexity of the control electronics when the number of tunable elements increases together with the PIC integration level, the amount of power that is consumed when the number of these components becomes large and crosstalk, with a potential loss of performance.

An alternative solution is a permanent modification of a waveguide structure, tailoring of guided mode properties which counterbalances the fabrication imperfections to achieve the desired device characteristics. This post-fabrication trimming (PFT) technique can provide a much simpler set-it-once-and-forget-it mechanism for adjusting photonic components, which is typically achieved by permanently changing the refractive index of either a core or cladding material of optical waveguides and, hence, does not require a constant supply of power.

Examples of trimming via a waveguide core modification include laser ablation [14], localized annealing of an ion implanted waveguide section [15], UV irradiation of hydrogenated amorphous silicon waveguide [16] and local oxidation by an atomic force microscope probe [17]. The first technique is universal and can be used for any material platform, however it is a rather destructive method with a damage of waveguide material and structure. The other techniques were developed for silicon photonics and cannot be directly applied for other substrate materials.

Trimming of waveguide cladding has been demonstrated via electron beam induced compaction and strain of silicon dioxide (SiO₂) [18], electron bleaching of chromophore-doped polymer [19], photodarkening of chalcogenide (A₂S₃) glass [20] and corrective etching of nitride films [21]. The additional cover layer is modified in this approach without affecting the waveguide core. Thus, these techniques are more universal and can be used for many material platforms. However, most of the proposed techniques suffer from the long-term stability problem. The level of the SiO₂ cladding compaction relaxes over time [22]. It is known that in the case of photo-sensitive polymers and chalcogenide glasses refractive index drifts over time due to densification [23] and structural relaxation [20], respectively. These effects cause a great deal of reliability concern for the proposed PFT

This work was supported by the Russian Science Foundation project 19-00511

Aleksandr Tronev, Mikhail Parfenov, Petr Agruzov, Igor Ilichev and Aleksandr Shamrai are with the Ioffe Institute, Saint Petersburg, 26 Polytechnicheskaya Street, Russia (e-mail: trone2008@ya.ru; mvparfenov@yandex.ru; piotrag@rambler.ru; iiv@mail.ioffe.ru; achamrai@mail.ioffe.ru).

Andrei Ionov, Sergey Bozhko, Rais Mozhchil and Sergey Chekmazov are with the Institute of Solid State Physics of the Russian Academy of Sciences, Chernogolovka, Moscow District, 2 Academician Ossipyan street, Russia (e-mail: bozhko@issp.ac.ru; ionov@issp.ac.ru; mr_mozhchil@mail.ru; chekmazov@issp.ac.ru).

techniques. Corrective etching of nitride films is very stable in time [21]. However, it is more suitable for reducing a random variation on the wafer level and cannot be directly applied for precise adjustment of individual components of PIC with real time monitoring of their characteristics.

In the previous works [24], [25] we demonstrated modification of a 5 nm thick titanium film on the top of a titanium in-diffused lithium niobate (Ti:LiNbO₃) waveguide by laser irradiation and supposed that this technique can be applied to a precise adjustment of the characteristics of integrated optical circuits.

In this paper we demonstrate the PFT technique based on local laser oxidation of a thin titanium film on the top of optical waveguides. The theoretical analysis has shown that a technique can be used for dielectric waveguide fabrication for different material platforms. We applied the proposed technique to improve the performance of a Mach-Zehnder modulator based on Ti:LiNbO₃ waveguides. A fine phase tuning with a step of 0.013 rad and extinction ratio (ER) enhancement up to 57 dB were demonstrated with a real time monitoring of the modulator transfer function. No long-term trimming relaxation was observed during several months of a periodical monitoring. The change in the effective waveguide refractive index and the available range of photonic device trimming will be even higher for the waveguides with a higher refractive index contrast and a smaller mode field diameter (MFD), such as those fabricated on the basis of thin-film lithium niobate (TFLN), silicon nitride or silicon on insulator (SOI).

II. THIN FILMS ON THE TOP OF DIELECTRIC OPTICAL WAVEGUIDES

The physical principals of the influence of a cover thin film on an optical waveguide can be explained by a simplified model of zigzag beam propagation in a four-layer waveguide structure (Fig 1) [24]. Changes in the waveguide effective refractive index and absorption coefficient due to light penetration into the thin film can be estimated in terms of the film reflection coefficient [26]:

$$\begin{aligned} \Delta n_{eff} &= \frac{\lambda}{2\pi} \cdot \frac{\phi_f}{2h \cdot \tan(\varphi)}, \\ \Delta \alpha &= \frac{1 - R_f}{2w \cdot \tan(\varphi)}, \end{aligned} \quad (1)$$

where λ is the light wavelength, h is the waveguide height, φ is the angle of beam propagation in the waveguide mode (a single mode waveguide is considered), R_f and ϕ_f are the amplitude and phase of the film complex reflection coefficient r_f , respectively. The film reflection results from the interference of reflection from waveguide/film and film/air interferences

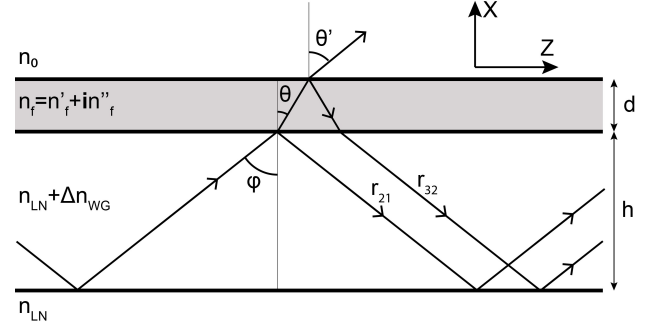


Fig. 1. Zigzag beam propagation in a four-layer waveguide structure.

$$\begin{aligned} r_f &= \sqrt{R_f} \exp(i\phi_f) = \frac{r_{32} + r_{21} \exp(i\delta)}{1 + r_{32}r_{21} \exp(i\delta)}, \\ \delta &= 2 \frac{2\pi}{\lambda} n_f d \cos \theta. \end{aligned} \quad (2)$$

Here r_{32} and r_{21} are the Fresnel reflection coefficients for waveguide-film and film-air interface respectively, the phase shift δ depends on the film thickness d and film refractive index $n_f = n'_f + in''_f$, which is a complex value in the general case. The qualitative analysis shows that the higher the film refractive index, the higher its influence on the optical waveguide. Note that the film thickness is restricted by the cutoff conditions of higher order modes.

A titanium metal film is a promising candidate for fine tuning of waveguide properties. It is characterized by a high real part of refractive index $n'_{Ti} = 3.68$ at 1550 nm [27] which is even higher than the silicon refractive index. Thus, it can be used for most of material platforms for the dielectric waveguide fabrication. A moderate imaginary part of refractive index $n''_{Ti} = 4.53$ [27] gives an acceptable excess optical loss for a properly chosen film thickness. Different influences on the TE and TM polarization waveguide modes due to plasmon polariton excitation [28] give a possibility of the light polarization control.

Titanium (Ti) is quite attractive from the technological aspect because of a CMOS compatibility. DC magnetron sputtering can be used for a high-quality deposition of films with stable optical characteristics which have a good adhesion to most materials of dielectric waveguides. A thin Ti film can be locally oxidized by laser illumination [29]–[32] which will be considered in detail in the next section. TiO₂ is a well-known material in integrated optics [33]. For example, it is used for hybrid waveguides on thin film lithium niobate [34], [35] and as a corrective layer for athermal silicon photonic devices [36]. This is also a very stable material with significantly different optical properties as compared with Ti. Thus, laser oxidation provides a way for a permanent laser trimming of PICs with a little additional space consumption.

A quantitative estimation of the effects of thin Ti and TiO₂ films on dielectric optical waveguides was carried out by using numerical simulation by the finite element method. Three material platforms for optical waveguide fabrication were considered. These were a Ti indiffused lithium niobate (Ti:LiNbO₃) waveguide [37], a thin-film lithium niobate (TFLN) waveguide in the form of an etched rib [38], and a silicon-on-insulator (SOI) waveguide [39]. The material platforms chosen represent three levels of refractive index

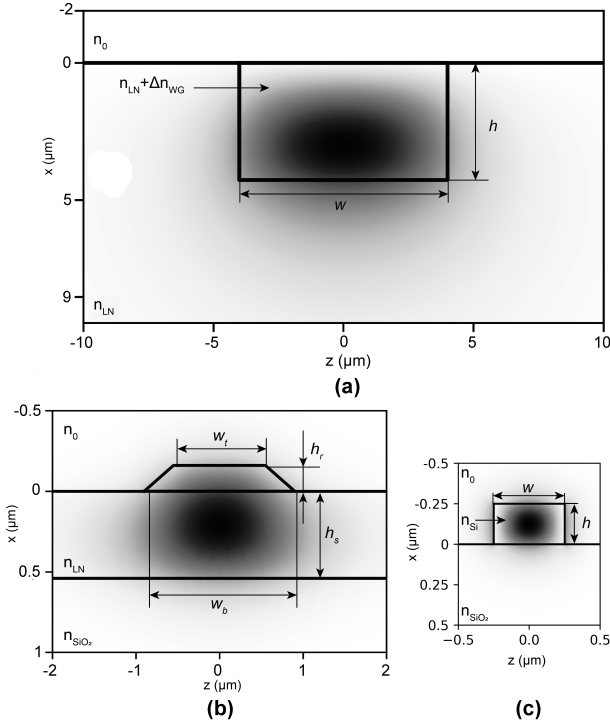


Fig. 2. Channel waveguide and calculated electric field distributions of TE modes used in the simulation for a Ti-indiffused lithium niobate (Ti:LiNbO₃) waveguide (a), a thin-film lithium niobate (TFLN) rib waveguide (b) and a silicon-on-insulator (SOI) waveguide (c).

contrast and MFD. In the case of Ti:LiNbO₃ waveguides, the refractive index contrast ($\sim 10^{-3}$) is low, and the mode is loosely confined (MFD $\sim 10 \mu\text{m}$). TFLN waveguides have a high refractive index contrast (~ 1) and tight mode confinement (MFD 1-2 μm). The SOI waveguides have the highest refractive index difference (~ 2) and the lowest MFD ($< 1 \mu\text{m}$). Other material platforms can be subsumed to one of these three levels of refractive index contrast and MFD.

We restricted ourselves to the analysis of a horizontally polarized (TE) waveguide mode which is used in electro-optic modulators. Note that the influence of a Ti film on the orthogonal TM mode can be higher due to the plasmon polariton mode excitation [28]. However, the light propagation conditions for very thin films (several nm thick) which as will be shown below are preferred for laser oxidation are far from the surface plasmon polariton mode excitation [40] and the Ti film influence on the TM mode is similar to the effect on the TE mode.

Typical parameters for single mode waveguides at wavelength 1550 nm were used in the analysis for each material platform and were presented earlier in experimental works [41]–[45]. To reduce the computational complexity, the Ti:LiNbO₃ gradient waveguide was replaced by step-index waveguides with width $w = 8 \mu\text{m}$, height $h = 4.5 \mu\text{m}$ and refractive index difference $\Delta n = 5 \times 10^{-3}$ [41] (Fig. 2a). The TFLN waveguide rib had width $w_r = 1.1 \mu\text{m}$ at the top and width $w_b = 1.8 \mu\text{m}$ at its base and height $h_r = 160 \text{ nm}$ [42] (Fig. 2b). The slab height was $h_s = 540 \text{ nm}$. For the waveguides directed along the y crystal axis on an x -cut LiNbO₃ single crystal substrate TE mode was an extraordinary wave. Thus, the extraordinary refractive index $n_e = 2.14$ was

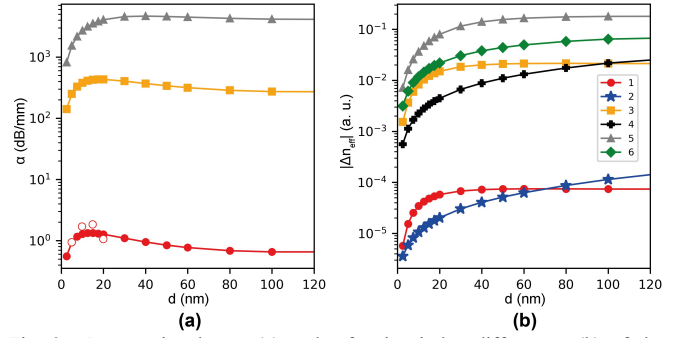


Fig. 3. Propagation losses (a) and refractive index differences (b) of the modes induced by the presence of Ti and TiO₂ layers of different thicknesses d on the waveguide top. 1 (circles) – Ti:LiNbO₃ with Ti layer (results of measurements of waveguide loss change per unit length at laser oxidation are shown as open circles); 2 (stars) – Ti:LiNbO₃ with TiO₂ layer; 3 (squares) – TFLN with Ti layer; 4 (crosses) – TFLN with TiO₂ layer; 5 (triangles) – SOI with Ti layer; 6 (rhombuses) – SOI with TiO₂ layer.

used. The SOI waveguide channel had the smallest sizes $w = 500 \text{ nm}$ and height $h = 250 \text{ nm}$ (Fig. 2c) [43]. The refractive indexes of silicon dioxide and silicon at wavelength of 1550 nm were set as $n_{\text{SiO}_2} = 1.44$ [44] and $n_{\text{Si}} = 3.48$ [45].

The simulation of waveguide modes was performed with the help of the COMSOL Multiphysics software package. The influence of metal Ti and dielectric oxidized Ti in the form of titanium dioxide (TiO₂, $n_{\text{TiO}_2} = 2.31$ [33]) films deposited on the waveguide top was investigated for the film thicknesses ranging from 2.5 to 100.0 nm. The absorption coefficient versus Ti film thickness is presented in Fig 3a. The Ti film induces a propagation loss which has a broad maximum for a maximal overlap between the conducting Ti layer and a waveguide mode field. As the loss induced by the Ti film grows, the effective refractive index decreases (Fig 3b) and the mode spot is slightly shifted in the substrate depth. The TiO₂ layer does not produce any loss but increases effective refractive indexes (Fig. 3b). The refractive index differences induced by the Ti and TiO₂ layers are lower than the contrast between the modal effective index and refractive index of the substrate. Thus, they do not provoke a leakage.

Comparison of the results obtained for different material platforms leads to the conclusion that the influence of Ti metal overlay on the waveguide mode properties is higher for the waveguides with a higher numerical aperture since they have a greater overlap between the cover layer and a waveguide mode field.

III. TITANIUM LASER OXIDATION

Laser oxidation of a thin Ti film was earlier used for the formation of micro- and nano- structures of diffractive elements [30]. The possibility of repeatable writing of the titanium dioxide line narrower than the diffraction limited focused laser spot [31], [32] was demonstrated. Thus, this technique looks very promising for photonic circuit trimming where a high resolution is required especially for the waveguides with a high numerical aperture, such as a SOI waveguide.

The physical mechanism of laser oxidation is as follows. Laser radiation is absorbed in the titanium film and causes a

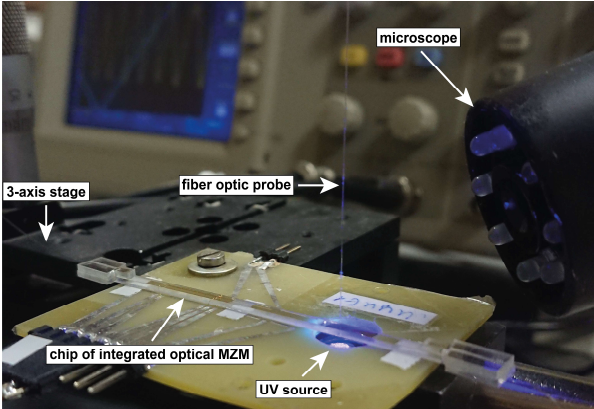
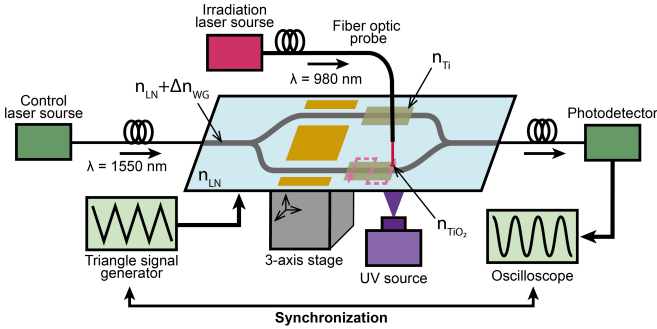


Fig. 4. Experimental setup for local Ti film laser oxidation.

local heating which depends on the laser power, spot size and thermal conductivity. The oxidation process is described by the Cabrera-Mott theory [46] as a migration of oxygen ions in the titanium oxide layer caused by an internal electric field (Mott potential) formed due to the excitation of titanium atoms. The excitation is highly dependent on local temperature. A higher optical power is required to provide local heating to a given temperature and to start the oxidation process for thicker films, which have a higher heat transfer coefficient. As oxidation progresses, two counteracting processes occur. On the one hand, as the oxide thickness grows the internal field decreases and the oxidation process slows. On the other hand, the metal thickness and the heat transfer coefficient decrease, which leads to a growth in the local temperature. Stable oxidation is observed as a balance between these processes. After a through-thickness oxidation of the transparent substrate occurs, the absorption of laser radiation sharply decreases, heating stops and the temperature drops, thus leading oxidation to a halt.

The set of samples was prepared for experimental investigations of the Ti film laser oxidation. Fused silica and *x*-cut congruent single crystal LiNbO₃ were used as substrates. Y propagated Ti:LiNbO₃ single mode (at 1550 nm) optical waveguides were produced on LiNbO₃ substrates. The Ti films of different thicknesses (5, 10, 15, 25 and 100 nm) were deposited on the substrate by DC magnetron sputtering.

Experimental investigations of laser oxidation of titanium films and the demonstration of PIC PFT were performed on the same setup (Fig. 4). A simple CW semiconductor pumping laser from an erbium doped fiber optic amplifier was used. The sample substrates had a low absorption at the laser wavelength 978 nm. Therefore, the laser irradiation mostly

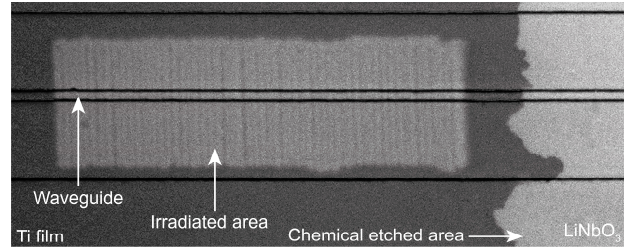


Fig. 5. Transparent traces on the metal Ti film after laser irradiation.

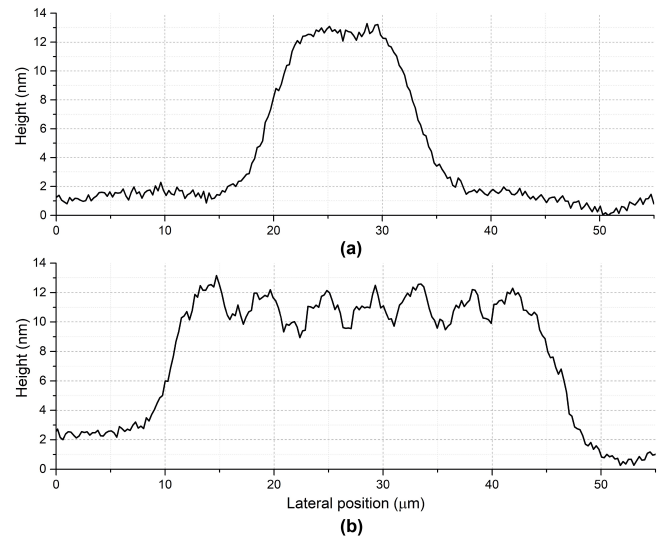


Fig. 6. The height profiles of the Ti film irradiated areas by single (a) and meander like path (b) probe movements.

affected the Ti films and did not influence on the substrate materials. Note that other substrate material platforms will require a different wavelength in order to oxidize Ti without the influence on the substrate. For instance, the SOI waveguides have a significant absorption at wavelength 978 nm, thus a longer wavelength should be used. It is convenient that the laser thermal Ti excitation used to start oxidation process can be realized in a wide wavelength range.

The output single mode fiber (PM980-HP) of the laser was exploited as a probe. The fiber tip was positioned close to a sample surface (at a height of about 50 μm). The laser spot was about 10 μm in diameter and the maximum peak intensity was about 1 kW/mm². The sample was attached to a precise 3-axis translation stage which provided the laser spot movement in a predetermined path on the sample surface. The speed of the fiber probe scanning was 1 mm/s. Like in the previous study devoted to laser Ti oxidation [30], [31] all the processes were carried out in air i.e., without a specific gas atmosphere.

First, the change in the Ti films morphology under laser irradiation was investigated. The stripes from the straight single path of the fiber probe and rectangular areas from the meander-like multi path of the fiber probe movement were formed by laser irradiation of the sample surface (Fig 5) [24]. The meander-like path with a half period of 5 μm was used to ensure path overlapping and oxidized rectangular areas continuity. The laser influence was seen in the form of transparent traces on the metal Ti film. The AFM images

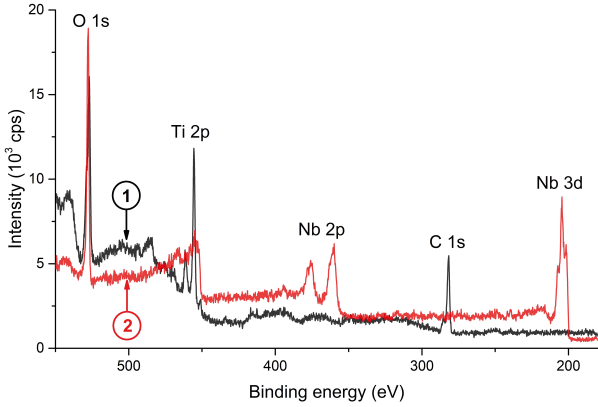


Fig. 7. XPS spectra of irradiated area of 5 nm Ti film. The black line (1) – spectrum from the top surface; the red line (2) – spectrum after 7 min of slow (~ 2 nm/min) etching and 4 min of fast (~ 20 nm/min) etching.

showed swelling in the laser irradiation area. The examples of height profiles of oxidation of a 5 nm thick Ti film on a LiNbO₃ substrate are shown in Fig. 6 [24]. The swelling height is about 13 nm. A periodic contour is seen on the top of rectangular areas. This is attributed to the meander-like path of the fiber probe scanning.

Then the composition of the films was studied by X-ray photoelectron spectroscopy (XPS). The lines related to titanium dioxide (TiO₂) in the XPS spectra of the irradiated areas indicated that the laser-induced Ti oxidation took place. The carbon line was attributed to surface contamination. The plasma etching was used for the investigation of the film composition change in the depth of the oxide film. XPS spectra of very thin films (5, 10 and 15 nm) did not alter with depth and titanium line (Ti 2p) disappeared after complete film removal from the substrates (Fig. 7). There is the evidence of homogeneous oxidation and an additional confirmation of a very weak effect on the substrate material. The results are well described by the physical model in which the oxidation of very thin Ti films starts at a relatively low temperature and stops quickly after through oxidation.

XPS spectra for the thicker film varied with the film depth (Fig 8). The change in the titanium line shape is related to the change in the oxidation degree, which decreased with the film depth. The XPS spectrum after a complete removal of the oxidized 100 nm Ti film from the LiNbO₃ substrate consisted of the line of the titanium traces related possibly to the Ti-indiffusion into the substrate. Apparently, after some threshold Ti film thickness the oxidation process began to affect the substrate material. Inhomogeneities and defects in the oxidized 20 nm Ti film were also observed on scanning electron microscope (SEM) images (Fig. 9). In accordance to the physical model, the film was locally heated to a higher temperature which potentially could lead to film defects and indiffusion into the substrate.

Finally the film influence on the Ti:LiNbO₃ waveguides was studied. As predicted by the theoretical analysis in section 2 the titanium film oxidation should reduce the optical loss. To investigate it, the rectangular areas of laser oxidation were intentionally produced over Ti:LiNbO₃ waveguides on the

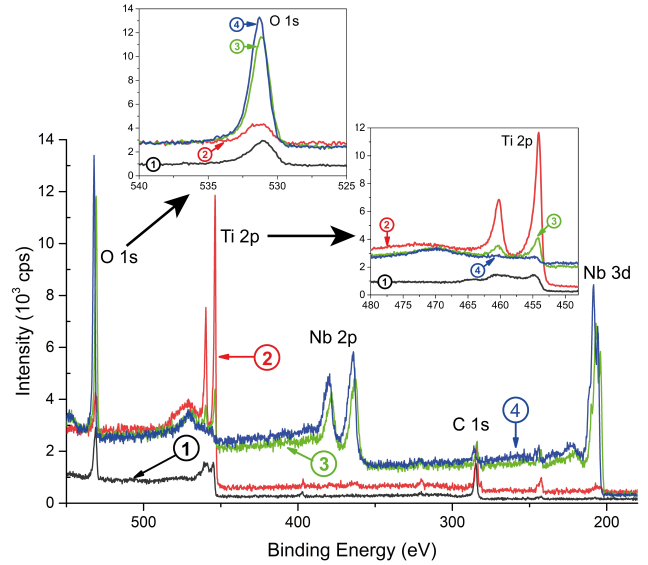


Fig. 8. XPS spectra of irradiated area of 100 nm Ti film at different ion etching times: the black line (1) – 4 min of slow etching, the red line (2) – 4 min of slow etching and 3 min of fast etching, the green line (3) – 4 min of slow etching and 11 min of fast etching, the blue line (4) – 4 min of slow etching and 18 min of fast etching.

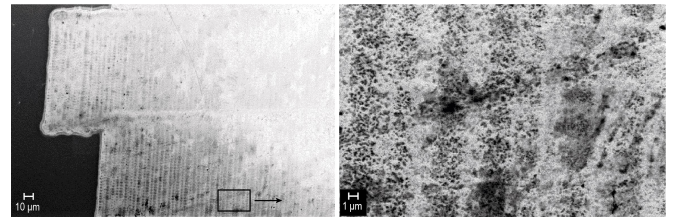


Fig. 9. SEM images with inhomogeneities and defects in the 20 nm titanium film after laser irradiation and through-thickness oxidation.

LiNbO₃ substrates. The input and output single mode optical fibers were attached to the optical waveguides for the optical loss real-time monitoring. The waveguide loss change per unit length was measured at laser oxidation during the meander path scanning of the fiber probe across the waveguide channels. The theoretical prediction was confirmed by the experimental dependence of the Ti metal overlay influence on the insertion loss of Ti:LiNbO₃ waveguide (Fig. 3a).

IV. MACH-ZEHNDER MODULATOR TRIMMING

The proposed technique of Ti film laser oxidation was used for the experimental demonstration of PFT of the LiNbO₃ Mach-Zehnder modulator (MZM). The samples of integrated optical MZM were fabricated on the *x*-cut congruent single crystal LiNbO₃ substrate (Fig. 4) by thermal titanium indiffusion. The light propagation was along the *Y* crystallographic axis. Two single mode fiber optic pigtailed were attached to the chip (5 mm × 50 mm × 1 mm) to input and output an optical signal using the end-fire coupling technique [47]. The total fiber-to-fiber loss was about 4.2 dB and they slightly varied from one sample to another. The 5 nm thick Ti was deposited over the waveguides in the area of two parallel arms clear of electrodes. It covered both waveguides and was 2 mm in length along the light propagation direction.

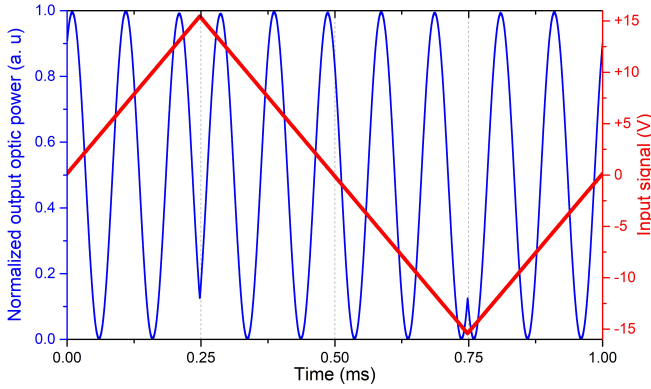


Fig. 10. On-line monitoring of the cosine MZM response to an input triangular signal.

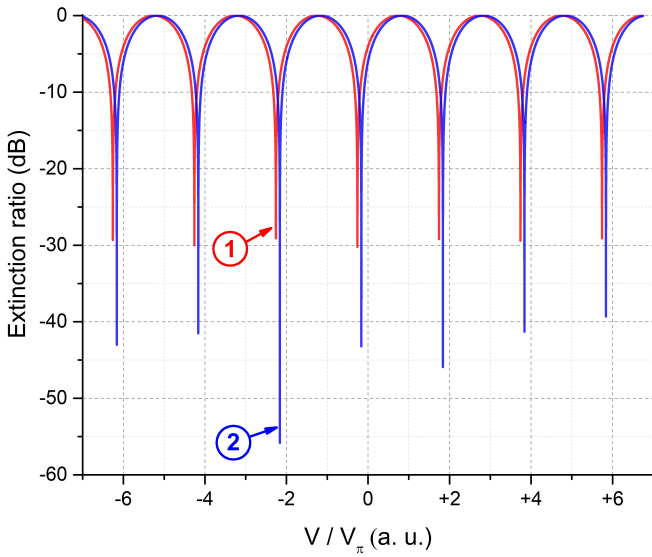


Fig. 11. Enhancement of extinction ratio in MZM: the MZM response before PFT (1) and after PFT (2).

The additional losses attributed to the Ti film were about 2 dB.

MZM trimming was performed on the same setup which was used for the experimental investigation of laser Ti film oxidation process (Fig 4). On-line monitoring of the modulator transfer function was carried out during the trimming process. A fiber pigtailed distributed feedback laser diode (DFB LD) with wavelength of 1550 nm and output power of 13 dBm was used as a signal light source. A triangular signal with a peak-to-peak voltage of 30 V which was 9 times higher than the modulator half-wave voltage ($U_\pi = 3.28$ V) was applied to the modulator from a signal generator, then it was detected by a p-i-n photodiode (PD) at the modulator output and displayed on a digital oscilloscope as a typical cosine function (Fig. 10). A homogenous illumination of the samples by low intensity (~ 1 mW/mm²) incoherent UV light was additionally applied from the chip bottom to suppress the photorefractive response of LiNbO₃ to laser irradiation [48] and ensure that only the Ti film oxidation affected the modulator.

Two types of the MZM adjustment were demonstrated. An improvement in the extinction ratio was achieved first. The initial extinction ratio of the samples was in the range 20 – 30

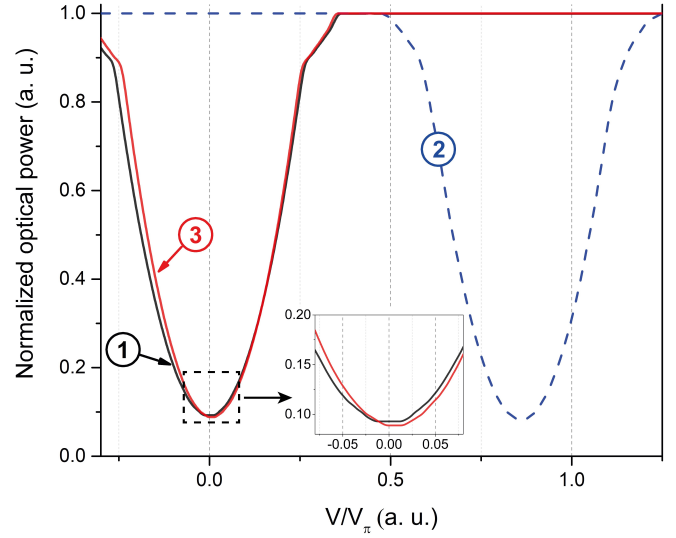


Fig. 12. Shift of a cosine transfer function minimum. The black line (1) shows the position before laser irradiation; the dotted blue line (2) is the phase shift just after Ti film laser irradiation (a single pass of the fiber probe across the waveguide); the red line (3) is the stable relative phase shift after the transition process for one zigzag pass (~ 10 μ m) across the waveguide in one of the MZM arms.

dB. The reduction in the optical loss caused by the Ti film oxidation was used for balancing the light intensity in the Mach-Zehnder interferometer arms by sequential illumination of different arms of the waveguide interferometer. On-line monitoring of the modulation contrast in the cosine electrooptic MZM response (transfer function) was used for a proper choice of the waveguide arm for the local laser oxidation and on-line termination of the fiber optic probe scanning (oxidation termination). The enhancement of the extinction ratio from 30 dB up to 57 dB was achieved (Fig. 11).

Note that the change in the cosine transfer function contrast was accompanied by the electrooptic response shift. A significant phase shift (about π) was observed in the first seconds after laser irradiation. Then the shift dropped rapidly to a stable value which did not change at a periodic monitoring during of several months. This effect was used for tuning the MZM operating point. A gradual tuning of the position of the cosine transfer function minimum was demonstrated (Fig. 12). The tuning step was about 4.07×10^{-3} V/V _{π} (0.0128 rad). It was corresponded to a single pass of the fiber probe across the waveguide and was defined by spatial resolution (laser spot size) which was about 10 μ m.

The initial significant phase shift occurred when the fiber probe was outside the optical waveguide. It grew as the probe moved toward the waveguide and then relaxed to a fixed value corresponding to the number of zigzag paths when the probe crossed the waveguide and moved away. This effect was observed only at laser irradiation of the Ti film-covered areas of the samples. In contrast to the reversible photorefractive phase shift [48], which also was observed at the irradiation of the waveguides without the Ti film, this phase shift could not be suppressed by homogeneous UV illumination of the

sample. Possibly, this behavior could be partially explained by a thermal response on the local high heating during Ti oxidation.

It should be also pointed up that the fixed phase shift was higher than that predicted by the theory which was attributed to the effective refractive index change caused by Ti oxidation. Additional investigations should be done to explain this result. Possibly, the mechanical stress caused by the TiO₂ overlayer plays a role.

Nevertheless, we emphasize again the stability of the MZM characteristics after adjustment which is a required feature of permanent PPT. The extinction ratio slightly decreased (by 3 dB) during the first week which can be attributed to a partial suppression of the photorefractive effect and a partial relaxation of the mechanical stress induced at laser oxidation. After that the maximum extinction ratio (57 dB) was stable at least during 4 months of the periodical monitoring. A long-period stability of the MZM operating point was difficult to trace because of a high influence of ambient conditions, first of all temperature.

V. CONCLUSION

In conclusion, a novel technique for post-fabrication trimming of photonic integrated circuits have been proposed. The technique is based on local laser oxidation of a thin Ti film. It can be applied for most of material platforms of dielectric optical waveguides and is CMOS compatible. The laser oxidation of Ti films effectively tunes both the absorption coefficient and effective refractive index of dielectric optical waveguides. Thus, versatile PFT of PICs can be realized. The investigation of local laser Ti film oxidation process showed that the technique has a very weak effect on substrate materials and can be classified as a technique of a cladding modification. The nonlinear mechanism of laser oxidation provides a high spatial resolution not restricted by a diffraction limited laser spot size, which is promising for PFT of the elements with a small footprint.

The efficiency of the technique was demonstrated as PFT of Ti:LiNbO₃ MZM. Lithium niobate is a rather complicated material for permanent PFT. It possesses many effects such as piezo, pyro, photorefractive and other effects which provide an additional mechanism of tuning on the one hand but are volatile and hinder on-line monitoring on the other hand. We used homogeneous UV illumination to suppress the effects related to space charge forming, in particular, the photorefractive effect. Fine tuning of the operating point and fixed extinction ratio enhancement up to 57 dB were demonstrated.

REFERENCES

- [1] Q. Cheng, M. Bahadori, M. Glick, S. Rumley, and K. Bergman, "Recent advances in optical technologies for data centers: a review," *Optica, OPTICA*, vol. 5, no. 11, pp. 1354–1370, Nov. 2018, doi: 10.1364/OPTICA.5.001354.
- [2] D. Marpaung, J. Yao, and J. Capmany, "Integrated microwave photonics," *Nature Photon*, vol. 13, no. 2, pp. 80–90, Feb. 2019, doi: 10.1038/s41566-018-0310-5.
- [3] V. M. N. Passaro, C. D. Tullio, B. Troia, M. L. Notte, G. Giannoccaro, and F. D. Leonardis, "Recent Advances in Integrated Photonic Sensors," *Sensors*, vol. 12, no. 11, Art. no. 11, Nov. 2012, doi: 10.3390/s121115558.
- [4] J. Wang, F. Sciarrino, A. Laing, and M. G. Thompson, "Integrated photonic quantum technologies," *Nat. Photonics*, vol. 14, no. 5, pp. 273–284, May 2020, doi: 10.1038/s41566-019-0532-1.
- [5] S. Y. Siew *et al.*, "Review of Silicon Photonics Technology and Platform Development," *Journal of Lightwave Technology*, vol. 39, no. 13, pp. 4374–4389, Jul. 2021, doi: 10.1109/JLT.2021.3066203.
- [6] D. Zhu *et al.*, "Integrated photonics on thin-film lithium niobate," *Adv. Opt. Photon., AOP*, vol. 13, no. 2, pp. 242–352, Jun. 2021, doi: 10.1364/AOP.411024.
- [7] T. Sharma *et al.*, "Review of Recent Progress on Silicon Nitride-Based Photonic Integrated Circuits," *IEEE Access*, vol. 8, pp. 195436–195446, 2020, doi: 10.1109/ACCESS.2020.3032186.
- [8] S. Mi, M. Kiss, T. Graziosi, and N. Quack, "Integrated photonic devices in single crystal diamond," *J. Phys. Photonics*, vol. 2, no. 4, p. 042001, Aug. 2020, doi: 10.1088/2515-7647/aba171.
- [9] L. Splitthoff, M. A. Wolff, T. Grottko, and C. Schuck, "Tantalum pentoxide nanophotonic circuits for integrated quantum technology," *Opt. Express, OE*, vol. 28, no. 8, pp. 11921–11932, Apr. 2020, doi: 10.1364/OE.388080.
- [10] M. Schell and D. de Felipe, "Polymer based photonic integration for sensors, communication, and active optical PCB," in *2017 IEEE CPMT Symposium Japan (ICSJ)*, Nov. 2017, pp. 185–188. doi: 10.1109/ICSJ.2017.8240112.
- [11] Y. Yamaguchi, S. Nakajima, A. Kanno, T. Kawanishi, M. Izutsu, and H. Nakajima, "High extinction ratio characteristics of over 60 dB Mach-Zehnder modulator with asymmetric power-splitting Y-branches on X-cut Ti:LiNbO₃," *Jpn. J. Appl. Phys.*, vol. 53, no. 8S2, p. 08MB03, Jul. 2014, doi: 10.7567/JJAP.53.08MB03.
- [12] J. E. Cunningham *et al.*, "Highly-efficient thermally-tuned resonant optical filters," *Opt. Express, OE*, vol. 18, no. 18, pp. 19055–19063, Aug. 2010, doi: 10.1364/OE.18.019055.
- [13] Q. Xu, S. Manipatruni, B. Schmidt, J. Shakya, and M. Lipson, "12.5 Gbit/s carrier-injection-based silicon micro-ring silicon modulators," *Opt. Express, OE*, vol. 15, no. 2, pp. 430–436, Jan. 2007, doi: 10.1364/OE.15.000430.
- [14] C.-C. Chen, H. Porte, J.-P. Goedgebuer, V. Armbruster, and R. Ferriere, "Adjustment of the coupling ratio by laser ablation of Ti:LiNbO₃ directional couplers," *Optics & Laser Technology*, vol. 34, no. 6, pp. 453–455, Sep. 2002, doi: 10.1016/S0030-3992(02)00041-5.
- [15] B. Chen *et al.*, "Real-time monitoring and gradient feedback enable accurate trimming of ion-implanted silicon photonic devices," *Opt. Express*, vol. 26, no. 19, p. 24953, Sep. 2018, doi: 10.1364/OE.26.024953.

- [16] T. Lipka, M. Kiepsch, H. K. Trieu, and J. Müller, "Hydrogenated amorphous silicon photonic device trimming by UV-irradiation," *Opt. Express, OE*, vol. 22, no. 10, pp. 12122–12132, May 2014, doi: 10.1364/OE.22.012122.
- [17] Y. Shen, I. B. Divliansky, D. N. Basov, and S. Mookherjea, "Electric-field-driven nano-oxidation trimming of silicon microrings and interferometers," *Opt. Lett., OL*, vol. 36, no. 14, pp. 2668–2670, Jul. 2011, doi: 10.1364/OL.36.002668.
- [18] J. Schrauwen, D. V. Thourhout, and R. Baets, "Trimming of silicon ring resonator by electron beam induced compaction and strain," *Opt. Express, OE*, vol. 16, no. 6, pp. 3738–3743, Mar. 2008, doi: 10.1364/OE.16.003738.
- [19] S. Prorok, A. Y. Petrov, M. Eich, J. Luo, and A. K.-Y. Jen, "Trimming of high-Q-factor silicon ring resonators by electron beam bleaching," *Opt. Lett., OL*, vol. 37, no. 15, pp. 3114–3116, Aug. 2012, doi: 10.1364/OL.37.003114.
- [20] A. Canciamilla *et al.*, "Photo-induced trimming of chalcogenide-assisted silicon waveguides," *Opt. Express, OE*, vol. 20, no. 14, pp. 15807–15817, Jul. 2012, doi: 10.1364/OE.20.015807.
- [21] A. H. Atabaki, A. A. Eftekhar, M. Askari, and A. Adibi, "Accurate post-fabrication trimming of ultra-compact resonators on silicon," *Opt. Express, OE*, vol. 21, no. 12, pp. 14139–14145, Jun. 2013, doi: 10.1364/OE.21.014139.
- [22] C. B. Norris and E. P. EerNisse, "Ionization dilatation effects in fused silica from 2 to 18-keV electron irradiation," *Journal of Applied Physics*, vol. 45, no. 9, pp. 3876–3882, Sep. 1974, doi: 10.1063/1.1663878.
- [23] C. G. Robertson and G. L. Wilkes, "Refractive index: A probe for monitoring volume relaxation during physical aging of glassy polymers," *Polymer*, vol. 39, no. 11, pp. 2129–2133, Jan. 1998, doi: 10.1016/S0032-3861(97)00508-9.
- [24] A. V. Tronev *et al.*, "Laser Modification of Titanium Film in Optical Waveguides on Lithium Niobate Substrates," *Tech. Phys. Lett.*, vol. 46, no. 9, pp. 885–888, Sep. 2020, doi: 10.1134/S1063785020090114.
- [25] A. V. Tronev *et al.*, "Direct Laser Modification of Thin Titanium Film for Fine-tuning of Photonic Lithium Niobate Circuits," in *2020 International Conference Laser Optics (ICLO)*, Nov. 2020, pp. 1–1. doi: 10.1109/ICLO48556.2020.9285720.
- [26] M. J. Adams, *An Introduction to Optical Waveguide*. Chichester ; New York: John Wiley & Sons Inc, 1981.
- [27] P. Johnson and R. Christy, "Optical constants of transition metals: Ti, V, Cr, Mn, Fe, Co, Ni, and Pd," *Phys. Rev. B*, vol. 9, no. 12, pp. 5056–5070, Jun. 1974, doi: 10.1103/PhysRevB.9.5056.
- [28] I. V. Il'ichev, N. V. Toguzov, and A. V. Shamray, "Plasmon-polariton polarizers on the surface of single-mode channel optical waveguides in lithium niobate," *Tech. Phys. Lett.*, vol. 35, no. 9, pp. 831–833, Sep. 2009, doi: 10.1134/S1063785009090132.
- [29] F. Xia *et al.*, "Mechanism of pulsed-laser-induced oxidation of titanium films," *Opt. Mater. Express, OME*, vol. 9, no. 10, pp. 4097–4103, Oct. 2019, doi: 10.1364/OME.9.004097.
- [30] Y. Wang *et al.*, "TiO₂ micro-devices fabricated by laser direct writing," *Opt. Express, OE*, vol. 19, no. 18, pp. 17390–17395, Aug. 2011, doi: 10.1364/OE.19.017390.
- [31] A. A. Gorbunov, H. Eichler, W. Pompe, and B. Huey, "Lateral self-limitation in the laser-induced oxidation of ultrathin metal films," *Appl. Phys. Lett.*, vol. 69, no. 19, pp. 2816–2818, Nov. 1996, doi: 10.1063/1.116853.
- [32] F. Xia, S. Li, K. Zhang, W. Kong, and M. Yun, "Analysis of the resolution enhancement in laser-induced TiO₂ nanostructured materials," *Opt. Mater. Express*, vol. 11, no. 1, p. 136, Jan. 2021, doi: 10.1364/OME.412870.
- [33] X. Guan, H. Hu, L. K. Oxenløwe, and L. H. Frandsen, "Compact titanium dioxide waveguides with high nonlinearity at telecommunication wavelengths," *Opt. Express, OE*, vol. 26, no. 2, pp. 1055–1063, Jan. 2018, doi: 10.1364/OE.26.001055.
- [34] S. Li, L. Cai, Y. Wang, Y. Jiang, and H. Hu, "Waveguides consisting of single-crystal lithium niobate thin film and oxidized titanium stripe," *Opt. Express, OE*, vol. 23, no. 19, pp. 24212–24219, Sep. 2015, doi: 10.1364/OE.23.024212.
- [35] T. Jin, J. Zhou, and P. T. Lin, "Mid-Infrared Electro-Optical Modulation Using Monolithically Integrated Titanium Dioxide on Lithium Niobate Optical Waveguides," *Sci Rep*, vol. 9, no. 1, p. 15130, Oct. 2019, doi: 10.1038/s41598-019-51563-5.
- [36] S. S. Djordjevic *et al.*, "CMOS-compatible, athermal silicon ring modulators clad with titanium dioxide," *Opt. Express, OE*, vol. 21, no. 12, pp. 13958–13968, Jun. 2013, doi: 10.1364/OE.21.013958.
- [37] M. Bazzan and C. Sada, "Optical waveguides in lithium niobate: Recent developments and applications," *Applied Physics Reviews*, vol. 2, no. 4, p. 040603, Oct. 2015, doi: 10.1063/1.4931601.
- [38] Y. Jia, L. Wang, and F. Chen, "Ion-cut lithium niobate on insulator technology: Recent advances and perspectives," *Applied Physics Reviews*, vol. 8, no. 1, p. 011307, Mar. 2021, doi: 10.1063/5.0037771.
- [39] S. Wu, X. Mu, L. Cheng, S. Mao, and H. Y. Fu, "State-of-the-Art and Perspectives on Silicon Waveguide Crossings: A Review," *Micromachines*, vol. 11, no. 3, Art. no. 3, Mar. 2020, doi: 10.3390/mi11030326.
- [40] H. Ditlbacher *et al.*, "Coupling dielectric waveguide modes to surface plasmon polaritons," *Opt. Express, OE*, vol. 16, no. 14, pp. 10455–10464, Jul. 2008, doi: 10.1364/OE.16.010455.
- [41] M. Parfenov, P. Agruzov, I. Il'tchev, and A. Shamray, "Simulation of Ti-indiffused lithium niobate waveguides and analysis of their mode structure," *J. Phys.: Conf. Ser.*, vol. 741, p. 012141, Aug. 2016, doi: 10.1088/1742-6596/741/1/012141.
- [42] A. J. Mercante, S. Shi, P. Yao, L. Xie, R. M. Weikle, and D. W. Prather, "Thin film lithium niobate electro-optic modulator with terahertz operating bandwidth," *Opt. Express, OE*, vol. 26, no. 11, pp. 14810–14816, May 2018, doi: 10.1364/OE.26.014810.

- [43] S. Xiao, M. H. Khan, H. Shen, and M. Qi, "Compact silicon microring resonators with ultra-low propagation loss in the C band," *Opt. Express, OE*, vol. 15, no. 22, pp. 14467–14475, Oct. 2007, doi: 10.1364/OE.15.014467.
- [44] I. H. Malitson, "Interspecimen Comparison of the Refractive Index of Fused Silica*,†," *J. Opt. Soc. Am., JOSA*, vol. 55, no. 10, pp. 1205–1209, Oct. 1965, doi: 10.1364/JOSA.55.001205.
- [45] H. H. Li, "Refractive index of silicon and germanium and its wavelength and temperature derivatives," *Journal of Physical and Chemical Reference Data*, vol. 9, no. 3, pp. 561–658, Jul. 1980, doi: 10.1063/1.555624.
- [46] N. Cabrera and N. F. Mott, "Theory of the oxidation of metals," *Rep. Prog. Phys.*, vol. 12, no. 1, pp. 163–184, Jan. 1949, doi: 10.1088/0034-4885/12/1/308.
- [47] V. Ramaswamy, R. C. Alferness, and M. Divino, "High efficiency single-mode fibre to Ti:LiNbO₃ waveguide coupling," *Electronics Letters*, vol. 18, no. 1, pp. 30–31, Jan. 1982, doi: 10.1049/el:19820022.
- [48] M. Parfenov, A. Tronev, I. Ilichev, P. Agruzov, and A. Shamrai, "Precise correction of integrated optical power splitters based on lithium niobate substrates by photorefractive effect local excitation," *Appl. Phys. B*, vol. 126, no. 5, p. 93, Apr. 2020, doi: 10.1007/s00340-020-07440-5.